Journal of Renewable Materials

Tech Science Press

DOI: 10.32604/jrm.2024.056970

ARTICLE

Experimental Study of Selective Batch Bio-Adsorption for the Removal of Dyes in Industrial Textile Effluents

Zakaria Laggoun[1,*], Amel Khalfaoui[1], Kerroum Derbal[2,*], Amira Fadia Ghomrani[3], Abderrezzaq Benalia[2,4] and Antonio Pizzi[5]

[1]Laboratory of Environmental Process Engineering (LIPE), Department of Environmental Engineering, Faculty of Engineering Process, University Salah Boubnider-Constantine 3, New City Ali Mendjeli, Constantine, 25000, Algeria

[2]Laboratory of Process Engineering for Sustainable Development and Health Products (GPDDPS), Department of Process Engineering, National Polytechnic School of Constantine, Constantine, 25000, Algeria

[3]Physics of Matter and Radiation Laboratory (LPMR), Department of Process Engineering, Faculty of Science and Technology, University Mohamed Cherif Messaadia, Souk Ahras, 41000, Algeria

[4]Higher Normal School of Constantine, Ali Mendjeli Nouvelle Ville, Constantine, 25000, Algeria

[5]Laboratoire d'Etude et Recherche sur le Matériau Bois (LERMAB), Ecole Nationale Supérieure des Technologies et Industries du Bois (ENSTIB), University of Lorraine, Epinal, 88000, France

[*]Corresponding Authors: Zakaria Laggoun. Email: zakaria.laggoun@univ-constantine3.dz; Kerroum Derbal. Email: derbal_kerroum@yahoo.fr

Received: 04 August 2024 Accepted: 25 October 2024 Published: 20 January 2025

ABSTRACT

This research aims to study the bio-adsorption process of two dyes, Cibacron Green H3G (CG-H3G) and Terasil Red (TR), in a single system and to bring them closer to the industrial textile discharge by a binary mixture of two dyes (TR+CG-H3G). The Cockle Shell (CS) was used as a natural bio-adsorbent. The characterizations of CS were investigated by Fourier transform infrared (FTIR), X-ray diffraction (XRD), scanning electron microscopy (SEM), energy-dispersive X-ray spectroscopy (EDX) and Brunauer–Emmett–Teller (BET). The adsorption potential of Cockle Shells was tested in two cases (single and binary system) and determined by: contact time (0–60 min), bio-adsorption dose (3–15 g/L), initial concentration (10–300 mg/L), temperature (22–61°C) and pH solution (2–12). The study of bio-adsorption (equilibrium and kinetics) was conducted at 22°C. The kinetic studies demonstrated that a pseudo-second-order adsorption mechanism had a good correlation coefficient ($R^2 \geq 0.999$). The Langmuir isotherm modeling provided a well-defined description of TR and CG-H3G bio-adsorption on cockle shells, exhibiting maximum capacities of 29.41 and 3.69 mg/g respectively at 22°C. The thermodynamic study shows that the reaction between the TR, CG-H3G dyes molecules and the bio-adsorbent is exothermic, spontaneous in the range of 22–31°C with the aleatory character decrease at the solid-liquid interface. The study of selectivity in single and binary systems has been performed under optimal operating conditions using the industrial textile rejection pH (pH = 6.04). CG-H3G dye is found to have a higher selectivity than TR in single (0–60 min) and binary systems with a range of 6–45 min, as shown by the selectivity measurement. It was discovered that CS has the capability to remove both CG-H3G and TR dyes in both simple and binary systems, making it a superior bio-adsorbent.

KEYWORDS

Cockle shells; bio-adsorption; binary system dyes; cibacron green; terasil red; selectivity

1 Introduction

Dyes can be described as intensely colored substances that have great solubility in water [1]. Dyes are pollutants widely used in food, paper, textile, and pharmaceutical industries, with an annual production of 7×10^5 tons [2].

Dyes are characterized by their ability to adsorb light in wavelengths between 380–750 nm [3]. This allows for the classification of synthetic dyes that are made from petrochemicals, as the most interesting type due to their great color diversity, water solubility, and ease of absorption compared to other dyes, such as natural dyes.

Organic dyes are a significant contributor to the organic pollutants in the environment, as stated in the World Bank's report [4]. Textile dyes have a negative impact on the aquatic environment of living organisms. They present many problems: they block the passage of light through water, thus reducing photosynthesis, changing ecosystem properties, and decreasing water quality (smell, color, and taste). Dyes in the water cause the percentage of oxygen to decrease in concentration, resulting in a decrease in the biological activity of the fauna and flora [5].

Several techniques are applicable to treat industrial color discharges such as coagulation [6], electrochemistry [7], electrocoagulation [8], electroseparation [9], photodegradation, membrane separation [10], electrodialysis [11], reverse osmosis [12], ion exchange [13], chemical precipitation [14], bioremediation, photocatalysis [15] and adsorption [16–18]. The adsorption process is a solution because of its simplicity, safety, abundance, and versatility in keeping these pollutants in check [19].

The coquette, this being a general term for small saltwater clams and marine bivalve molluscs of the Cardioid family [20], can be utilized as a cheap and effective adsorbent material [21]. The cockle shell's performance in removing organic and inorganic matter from polluted water has been found to be excellent [22].

Inorganic materials like calcium carbonate can be produced by biological systems, which have different structures, morphology, and polymorphisms. Calcium carbonate and organic components, such as anionic proteins and glycoproteins, are the main components of biological systems observed in many marine organisms, such as oyster shells, corals, ivory sea urchins, and bivalve molluscs [23].

The current research focuses on cockle shells which contain approximately 98%–99% calcium carbonate [24]. $CaCO_3$ is a material that can be used in many ways by humans. It is found in three main phases: Aragonite, Calcite, and Veterite. Chemically, the three forms are identical, but they differ in other aspects like homogeneity, whiteness, purity, and thickness. $CaCO_3$ can be either mined or chemically synthesized in the laboratory, and is widely used in many industrial applications as biomaterials for tissue engineering applications, such as drug delivery systems, bone tissue engineering, and bone networks [25].

The challenge of current research in Algeria is how to eliminate or reduce the percentage of colored pollution in national textile industries. Because the effluent has a mixture of dispersed dyes such as TR and reactive dyes such as CG-H3G, the concentration of chemical oxygen demand (COD) ranges from 250 to 300 mg/L.

In this study, cockle shells were used as bio-sorbents because of their high availability on Algerian beaches to eliminate the toxic dyes Terasil Red (TR) and Cibacron Green (CG-H3G) present in textile effluents of Algeria by using the bio-sorption process in both single and binary systems. The adsorption processes were optimized and modeled by studying the kinetic, thermodynamic, and influence parameters of the bio-sorption process.

2 Materiel and Methods

2.1 Preparation of Stock Solution

The stock solution of Terasil Red (TR) and Cibacron Green H3G (CG-H3G) was made by dissolving 1 g of Terasil Red and Cibacron Green-H3G in a volume of distilled water (V = 1000 mL). To achieve a concentration of equal to 1 g/L, the physicochemical proprieties of dyes TR and CG-H3G are presented in the Table 1.

Table 1: Physicochemical properties of dyes TR and CG-H3G

Properties	Terasil Red (TR)	Cibacron Green H3G(CG-H3G)
Dye index number	Disperse Red 349	Derived from RG 12
Molecular formulae	$C_{23}H_{21}Cl_2N_5O_5$	Indefinite (derived from RG 12)
Molecular weight (g/mol)	518.351	Indefinite (derived from RG 12, 1837.7)
Wavelength (nm)	521.4	672.2

2.2 Preparation of Cockle Shell as a Bio-Adsorbent

Cockle shells were gathered in the Djenah Jijel region of Algeria. The cockle shell adsorbent was made by several steps, including cleaning the cockle shells multiple times with distilled water to remove dust and then importing them. They were left to dry in air for 24 h. A brand grinder crushed the samples after drying. The sieving step was done to obtain a fine powder with a particle diameter ($d \leq 125$ µm) [17]. The recovered powder was used in the Terasil Red (TR) and Cibacron Green (CG) dyes bio-adsorption process [17].

2.3 Instrumental Characterization of Cockle Shell Powder

The purpose of characterizing Cockle shells is to provide information on functional groups, morphology and composition of biosorbent: FTIR was used to determine the functional groupings of the solid surface of CS in the range of 400–4000 cm^{-1} using the JASCO FT/IR 4600 instrument. The PHASER-BRUKER X-ray diffractometer was used to perform XRD analysis (XRD) in a 20–80° interval. The CS powder sample's morphological structure was determined using SEM. EDX analysis was used to determine the chemical composition of the sample using the THERMO FISHER QUATTROS instrument. Finally, the BET analysis to determine the area of the biosorbent was carried out using a Quantachrome® ASiQwin instrument version 5.21.

2.4 Batch Adsorption Studies

The CS adsorption study for Terasil Red (TR) and Cibacron Green (CG) dyes involved weighing 1 g of CS in 100 mL Erlenmeyer vials with different concentrations (10–300 mg/L). The initial solution had a pH_{TR} = 6.58 and $pH_{CG\text{-}H3G}$ = 8.25. The adsorption experiment took place in conditions of W = 300 RPM, T = 22°C and a predefined period. At a known initial adsorbate concentration, each time *t*, the spent CS was filtered using a brand centrifuge (HETTICH ROTOFIX 32A) and the TR concentration in the supernatant was measured by UV spectrophotometer (JASCO V-750). The adsorption capacity q_t ($mg.g^{-1}$) and elimination percentage (%) were calculated using the following equation [26]:

$$q_t = \left(\frac{C_0 - C_t}{m}\right) \times V \tag{1}$$

$$R(\%) = \left(\frac{C_0 - C_t}{C_0}\right) \times 100 \tag{2}$$

where C_0 and C_t are the solute concentrations (mg/L) at $t = 0$ and at time t, q_t (mg/g): solute adsorption capacity at time t, m: mass of adsorbent (g) and V represents the volume of aqueous solution to be treated (0.1 L).

3 Results and Discussion

3.1 Characterization of Bio-Adsorbent

3.1.1 FTIR Analysis

The main purpose of using FTIR spectrometry is to determine the functional groups on the shell's solid surface. CS powder FTIR analysis before and after TR and CG dyes bio-adsorption is shown in Fig. 1.

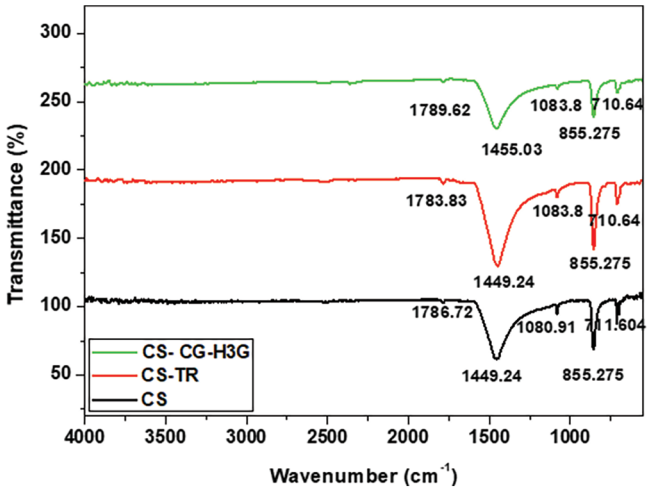

Figure 1: FTIR analysis of CS powder before and after adsorption TR and CG, adapted with permission from Reference [17], Copyright © 2023, MDPI Publishing

The powder cockleshell bands are visible in Fig. 1, with maximum values of 711.6, 855.27, 1080.91, 1449.24 and 1786.72 cm^{-1}. After the adsorption of the TR and CG-H3G dyes, a slight shift in the position of certain peaks was observed, but no change in structure was observed due to the appearance or disappearance of other peaks. The preservation of the physicochemical properties [27] of the CS adsorbent after TR adsorption may be attributed to this.

The presence of the peak at 711.6 cm^{-1} confirms the structural change of calcium ions from the symmetry of the calcite phase by dual degenerate planar bending mode (V_4); this peak also confirms the aragonite stage [28]. The inert carbonate ions (CO_3^{2-}) in the aragonite part [29] are designated to the out-of-plane bending mode (V_2) and its symmetric stretching mode (V_1) and V_1 is represented by the peaks at 855.27 and 1080.91 cm^{-1}, respectively.

The significant peak observed at 1449.24 cm^{-1} can be attributed to a structural alteration in the symmetry of the aragonite phase, which arises from the vibration mode associated with the double degenerated planar asymmetric stretch mode (V_3). Alternatively, this peak may also indicate the presence of alkyl groups within the polymorphic aragonite phase [24]. Furthermore, the peak located at 1786.72 cm^{-1} serves as definitive evidence of a single crystalline domain within the aragonite phase. This observation further substantiates the fundamental alterations in the positions of the vibrational modes of the sample, which are a consequence of modifications in the electrostatic valence of the CaO bond, resulting from changes in the surrounding oxygen atoms [24].

3.1.2 X-Ray Diffraction Analysis (XRD)

Fig. 2 shows that the cockleshell powder has a single phase of aragonite-shaped calcium carbonate, which agrees with the reference code, file [96-901-6718]. The CS powder has several peaks with the following 2-theta positions: 26.23, 27.16, 31.12, 33.10, 36.12, 37.89, 38.61, 41.11, 45.80, 48.39, 50.27, 52.25, and 52.97. These 2-theta positions correspond to the following crystal planes: (111), (021), (002), (012), (102), (112), (022), (211), (220), (221), (041), (132), (113), and (231). The largest peak at 26.23° and the crystalline plane (111) represents the aragonite-shaped calcium carbonate component.

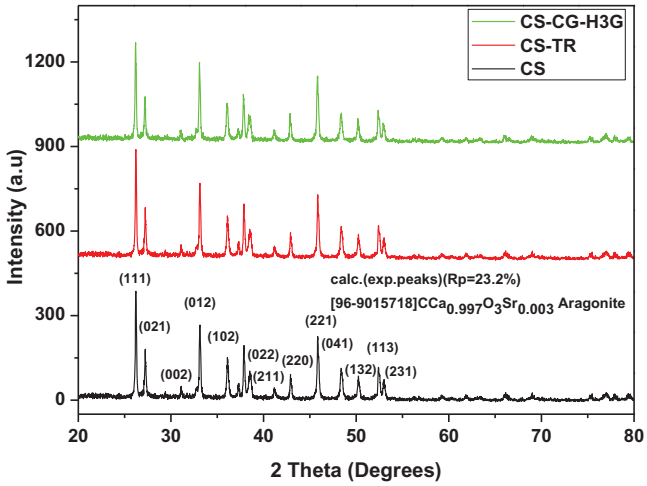

Figure 2: X-ray diffraction analysis (DRX) of CS powder before and after adsorption TR and CG-H3G, adapted with permission from Reference [17], Copyright © 2023, MDPI Publishing

According to Fig. 2, there is no change in the order, appearance and disappearance of peaks. The cockleshell adsorbent retains their physicochemical property before and after TR and CG-H3G dye adsorption.

Scanning electron microscopy (SEM) and energy-dispersive X-ray (EDX) analysis (Fig. 3a) shows that the structure of the CS powder is non-uniform and has an irregular shape. Fig. 3b,c shows that the dyes TR and CG molecules were fixed on the surface of the adsorbent.

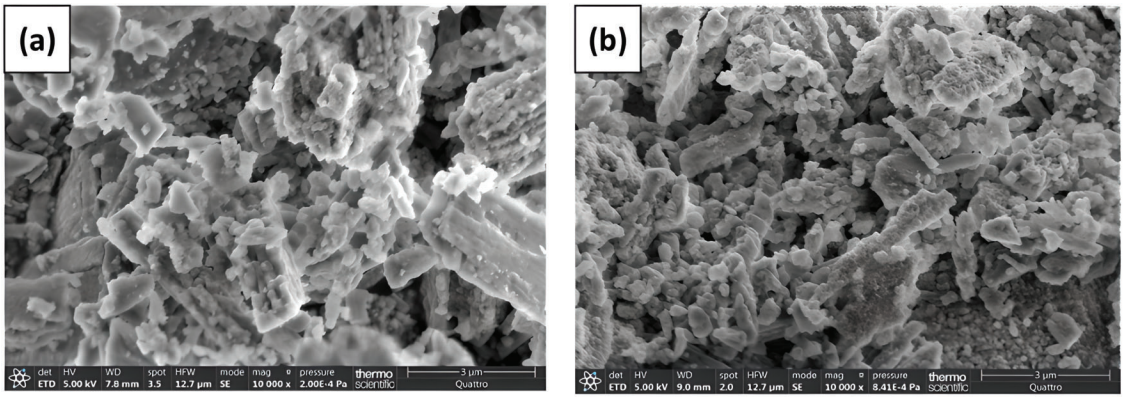

Figure 3: (Continued)

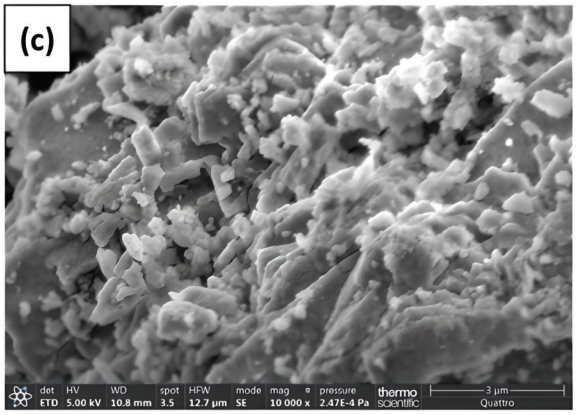

Figure 3: SEM of CS powder (a) before and after (b) TR and (c) CG-H3G adsorption, adapted with permission from Reference [17], Copyright © 2023, MDPI Publishing

Fig. 4a shows that the adsorbent contains the following atoms: oxygen (50.23%), calcium (31.48%), carbon (18.18%), and Strontium (0.1%), which indicates one component, namely calcium carbonate, more exactly aragonite, which is characterized by the presence of low proportions of strontium.

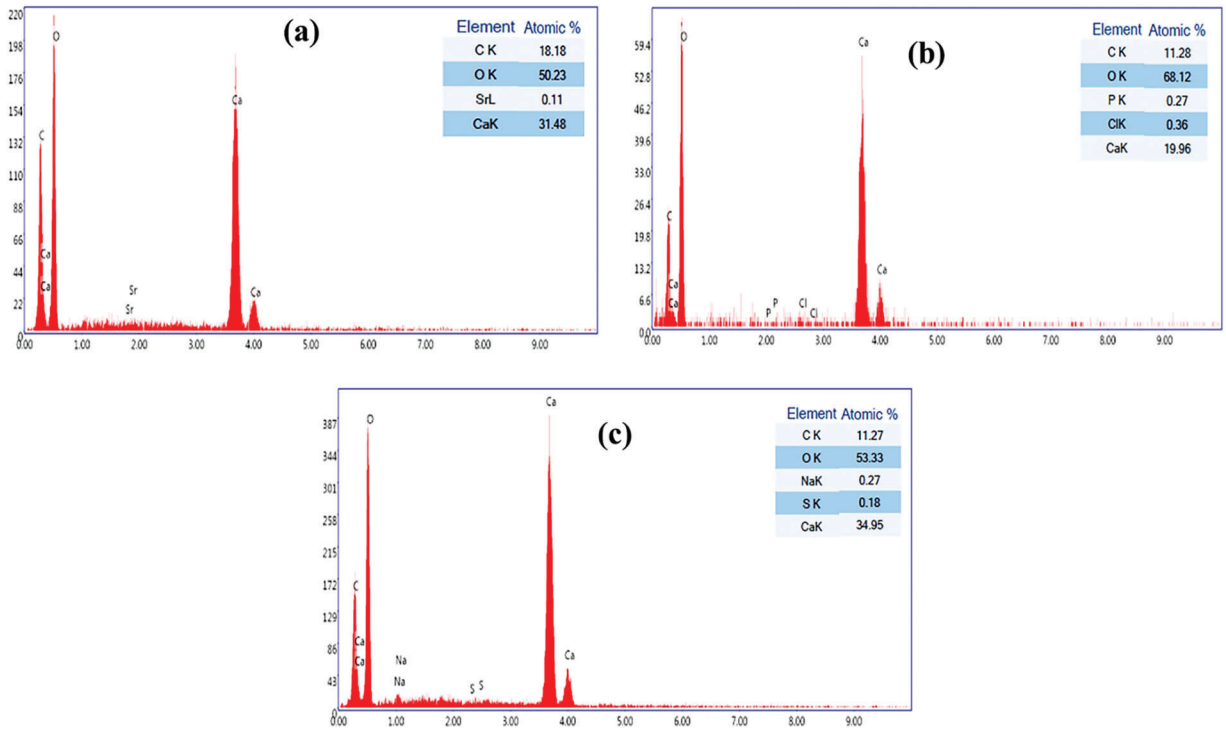

Figure 4: EDX of CS powder (a) before and after (b) TR and (c) CG-H3G adsorption, adapted with permission from Reference [17], Copyright © 2023, MDPI Publishing

The two Figs. 4b, 4c respectively show the percentages of atoms present after the bio-adsorption process of TR and CG-H3G dyes. A change in the percentages of calcium carbonate atoms with the disappearance of the percentage of strontium atoms can be noticed. The TR dye adsorption process was confirmed by the

appearance of phosphorus (0.27%) and chlorine (0.36%) atoms. The bio-adsorption of CG-H3G was also confirmed by the appearance of sodium (0.27%) and sulfur (0.18%).

3.1.3 Brunauer Emmet Teller (BET)

The linear form of BET is applicable for relative pressures (P/P_0) between 0.05 and 0.3, and is presented in the following form [30]:

$$\frac{\frac{P}{P_0}}{V\left(1-\frac{P}{P_0}\right)} = \frac{1}{V_m C} + \frac{C-1}{V_m C}\left(\frac{P}{P_0}\right) \tag{3}$$

V_m and C are calculated from the slope and the ordinate of the origin of the straight line $P/V\,(1-P) = f\,(P/P_0)$. The specific surface area of solid biomaterials can be calculated by the following equation:

$$S_{BET} = \frac{n_m N_A \sigma_m}{m} = \frac{V_m N_A \sigma_m}{V_{mol} m} \tag{4}$$

With σ_m: Molecular cross-section occupied by the nitrogen molecule (16.2A°2); m: Mass of biomaterial; V_{mol}: Molar volume of nitrogen gas under normal conditions (22.414 L/mol); N_A: Avogadro number (6.023 10^{23}mol^{-1}).

Fig. 5 shows the linear BET form of N_2 adsorption for cockle shells at a temperature of 77 K:

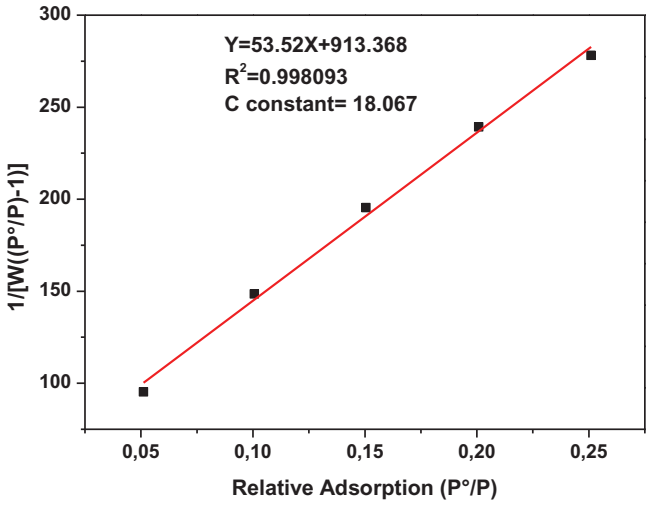

Figure 5: The linear form of N_2 adsorption BET for cockleshell (CS)

From the linear form in Fig. 5 and extracting it from constant C and applying it to Eq. (5), we obtain the specific cockleshell surface area S_{BET} = 3.603 m^2/g.

3.2 Parameters for the TR and CG Bio-Adsorption Study Onto Cockleshell (Single System)

3.2.1 Effect of Contact Time

The contact time is an important effect for understanding the adsorption phenomenon, and it controls the bio-adsorption kinetics from the start of adsorption until the bio-adsorbent saturation time [31].

Fig. 6 shows that the adsorption process of the two dyes goes through two stages. The first stage starts from 0 to 6 min, and represents rapid adsorption, which is due to the availability of active sites and the increase in the exchange area between the bio-adsorbent (CS) and the TR and CG-H3G dyes [28]. The

second stage (t > 6 min) is a slow adsorption, in which the adsorption capacity is relatively constant, and this being either due to the saturation of active sites or to the repulsive forces between the dye molecules on the surface of the CS bio-adsorbent [28], as was also shown. The adsorption capacity of the dye TR is greater than that of CG-H3G, and from this, we conclude that the TR dye is more selective than CG-H3G onto CS bio-adsorbent.

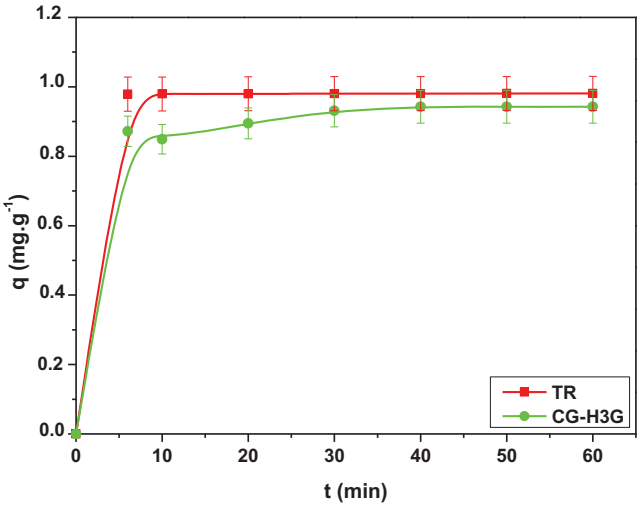

Figure 6: Effect of contact time on adsorption capacity of TR and CG-H3G dyes onto CS (C_0 = 10 mg/L, T = 22°C, r = 10 g/L, W = 300 rpm)

3.2.2 Effect of Bio-Adsorbent Dose

The effect of the biosorbent dose is more important for understanding the phenomenon of transfer of the solute in the aqueous phase to the solid surface of the bio-adsorbent [32]. The experiments were performed for an initial concentration of TR equal 10 mg/L. The adsorbent dose was varied between 3 and 15 g/L. Fig. 6 represents the percentage removal of TR and CG-H3G as a function of different doses of CS.

The presence of the two parts can be seen in Fig. 7. The first part represents the increasing proportion of the percentage of dye elimination TR (77%–98%) and CG-H3G (63.29%–94.25%) with an increased bio-adsorbent dose in range (3–10 g/L). This can be explained by the availability of a significant number of active sites [27]. The second part when the bio-adsorbent dose (r > 10 g/L) represents the percentage stabilization part of dye elimination CG-H3G (94.25%–94.35%), also represents the percentage reduction part for dye TR (98%–94.98%). The stabilization and or reduction in elimination percentage can be attributed to the saturation of the active sites of the bio-adsorbent CS [29].

3.2.3 Effect of Initial Concentration

The initial concentration effect of the TR and CG-H3G dyes on the adsorption by CS was obtained by varying the initial concentration of 10–300 mg/L. Fig. 8 shows the variation of the TR and CG-H3G adsorption capacity per CS as a function of time at different concentrations.

As shown in Fig. 8, the adsorption capacity gradually increases from 0.981 to 25.37 mg/g for the TR dye and from 0.942 to 3.64 mg/L for the CG-H3G one, when the initial concentration of TR and CG-H3G increases from 10 to 300 mg/L. This increase can be attributed to the increase in the driving force, which leads to a decrease in the resistance of the dye between the aqueous phase and the solid [33].

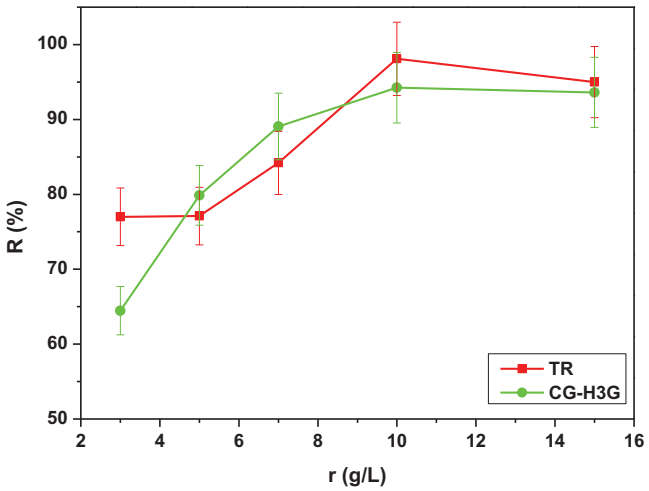

Figure 7: Effect of different doses of bio-adsorbent on adsorption capacity of TR and CG-H3G dyes onto CS ($C_{0\ TR,\ CG\text{-}H3G}$ = 10 mg/L, T = 22°C, W = 300 rpm)

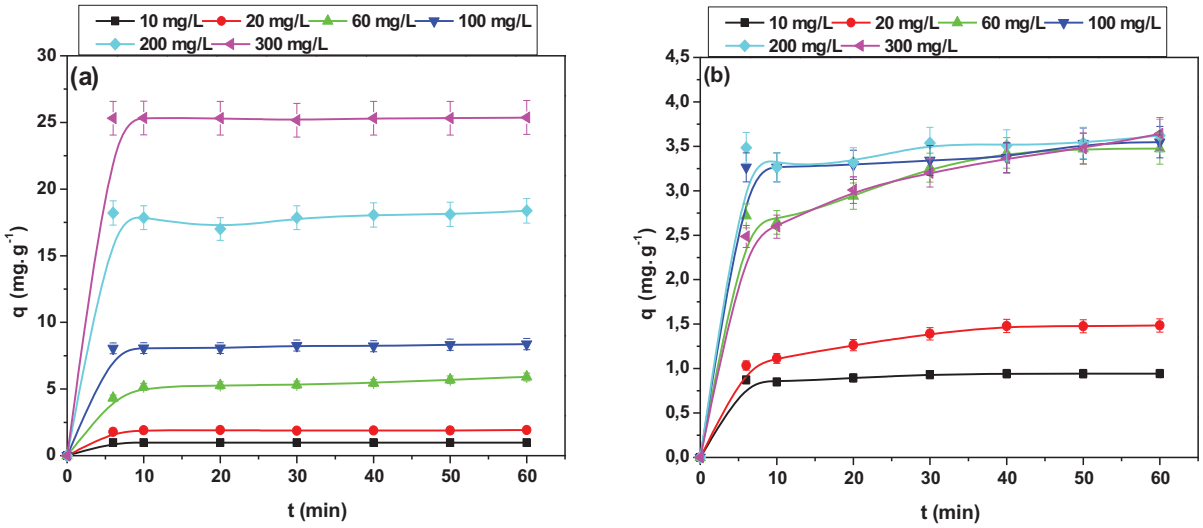

Figure 8: Effect of initial concentration on adsorption capacity of: (a) TR and (b) CG-H3G dyes onto CS (T = 22°C, r = 10 g/L, W = 300 rpm)

3.2.4 Effect of Temperature

This effect directly influences the movement of dye molecules in aqueous solutions and controls the degree of resistance of the bio-adsorbent for different temperatures.

Fig. 9 represents the effect of temperature on the adsorption capacity of the TR and CG-H3G dyes onto the CS powder in the range of 22°C to 61°C. It is noted, for the TR dye, the increase in temperature from 22°C to 61°C results in a decrease in the adsorption capacity from 0.981 to 0.455 mg/L. For the CG the increase in the temperature from 22°C to 31°C promotes the increase in the adsorption capacity from 0.942 to 0.956 mg/L. Conversely, when the temperature increases in the range from 31°C to 61°C, there is a decrease in the adsorption capacity of the CG-H3G dye from 0.956 to 0.838 mg/L. The increase in temperature accompanied by the increase in the absorption capacity of the dye may be because at higher temperatures the mobility of the dye molecules increases [34]. The increase in temperature from 31 to 61° accompanied by the decrease in the adsorption capacity of CG-H3G dye may be attributed by

breaking the bonds between the molecules of dye and the surface of the CS. An alternative explanation might be that the active sites are damaged by the rising temperature [35].

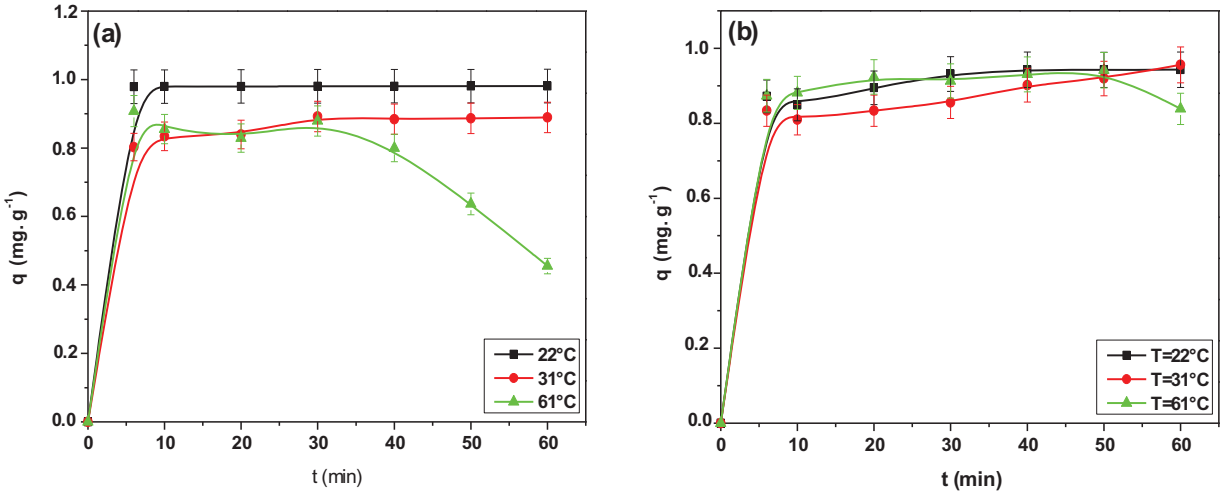

Figure 9: Effect of temperature on adsorption capacity of: (a) TR and (b) CG-H3G onto CS powder ($C_{0\ TR,\ CG\text{-}H3G}$ = 10 mg/L, r = 10 g/L, W = 300 rpm)

3.2.5 Effect of pH

The pH plays a crucial role in the adsorption process by simultaneously influencing the charge of the adsorbent and the pollutant. For this reason, we carried out a study of pH variation in the range 2 to 12. The pH was adjusted by adding a solution of sodium hydroxide NaOH (0.1–1 M) and hydrochloric acid HCl (0.1–1 M).

It should be noted that the TR is a disperse (non-ionic) dye. This disperse dye cannot be dissolved in water. When incorporated into aqueous solutions, it acts as an anionic dye in acidic media [36], and acts as a cationic dye in basic media. For this reason, there is a disturbance and minimal variation in adsorption capacity in the pH range from 2 to 12. This observation is followed by a maximum capacity in both very acidic and very basic media (pH = 12), as shown in Fig. 10a.

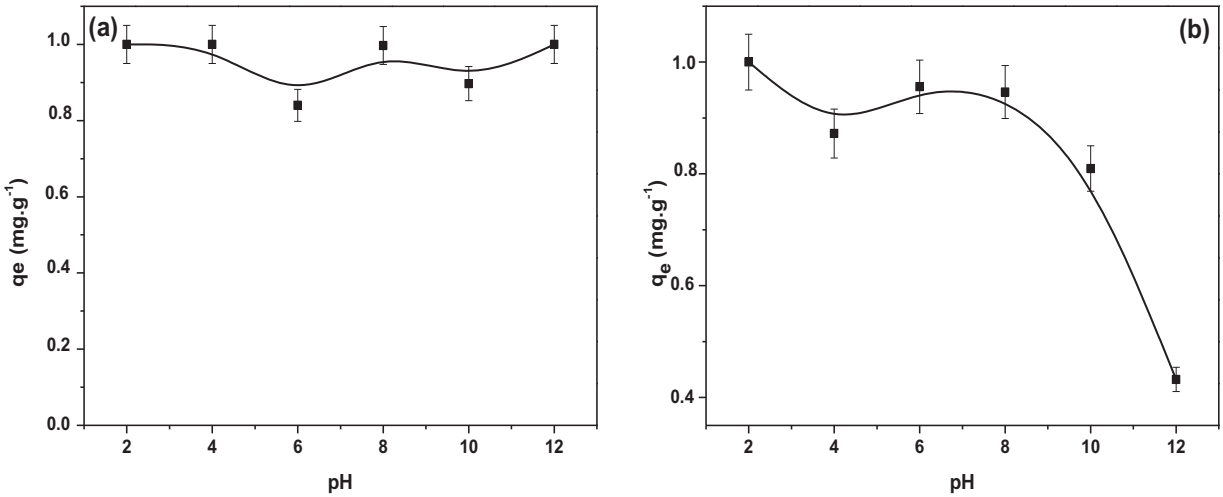

Figure 10: Effect of pH on adsorption capacity of: (a) TR and (b) CG-H3G onto CS powder ($C_{0\ TR,\ CG\text{-}H3G}$ = 10 mg/L, r = 10 g/L, W = 300 rpm)

Fig. 10b shows a decrease in the adsorption capacity of CG-H3G, which can be attributed to the difference in charge. In acidic environments, adsorption capacity is highest at pH = 2, as attractive forces create a bond between the negative charge of the dyes and the positive sites of the bio-adsorbent [37]. In a basic medium, increasing the degree of basicity will lead to an increase in hydroxide ions, with a minimum adsorption capacity of 12. This is when the differences in reputation are greatest between CG-H3G molecules and the negative sites of the bio-adsorbent CS [38].

3.3 Kinetic Adsorption

Kinetic studies are more important for understanding the mechanisms of adsorption of Terasil Red and Cibacron Green H3G dyes onto cockle shells. In this study, the following kinetic models were used: pseudo first order (PFO), pseudo second order (PSO) and inter-particle diffusion (IPD) model. The kinetic model and parameters are illustrated in Table 2. Fig. 11 shows the linear plot of PFO, PSO and IPD.

Table 2: The kinetic models and their nonlinear, linear, parameter, and plot forms

Adsorption kinetics	Parameters	Linear form	Plot	Ref.	Eq. No.
Pseudo-first-order (PFO) $q_t = q_e.e^{-k_1 t}$	k_1 (min^{-1}) q_e ($mg.g^{-1}$)	$Ln\ q_t = Ln\ q_e - k_1 t$	$Ln\ q_t$ vs t	[39]	(5)
Pseudo-second-order (PSO) $q_t = -\frac{k_2.q_e^2.t}{(1 + k_2.q_e.t)}$	k_2 ($g.mg^{-1}.min^{-1}$) q_e ($mg.g^{-1}$)	$\frac{t}{q_t} = \left(\frac{1}{q_e}\right)t + \frac{1}{k_2 q_e^2}$	$\frac{t}{q_t}$ vs t	[39]	(6)
Intra-particular Diffusion (IPD)	K_{id} ($mg/g.min^{0.5}$) C_{id} ($mg.g^{-1}$)	$q_t = k_{id}.t^{0.5} + C$	q_e vs $t^{0.5}$	[40]	(7)

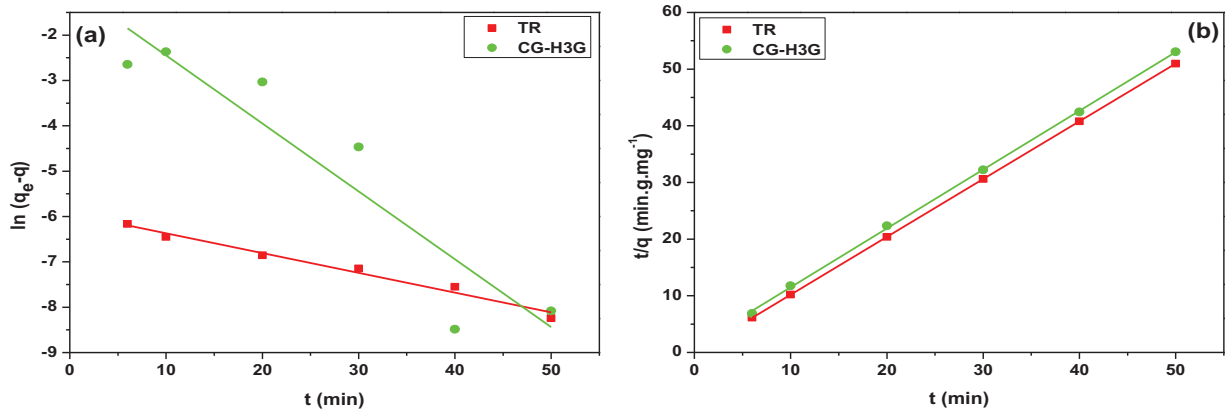

Figure 11: (Continued)

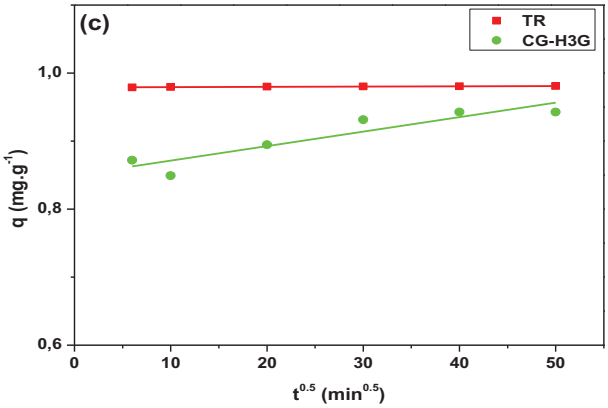

Figure 11: Linear plots: (a) PFO, (b) PSO and (c) IPD

Table 3 shows that the pseudo second order correlation coefficient is greater than the pseudo first order and is close to one. In addition, there is a convergence between the experimental adsorption capacity and the adsorption capacity calculated by the pseudo second-order kinetic model. Therefore, the pseudo second order model is the most suitable model to present the process of TR and CG-H3G bio-adsorption by cockleshells. The intra-particular diffusion kinetic model was used to investigate the mechanism of adsorption of the TR and CG dyes removal from their aqueous solutions using CS as a bio-adsorbent. Generally, internal or external mass transfer or both govern the adsorption process. According to Table 3, the constant ($C_{id} > 0$) noted the presence of the intergranular diffusion mechanism [26] of the TR and CG-H3G dye molecules onto CS powder.

Table 3: Results of PFO, PSO and IPD kinetic models

Dyes	PFO			PSO			IPD		
	k_1 (min^{-1})	q_e ($mg.g^{-1}$)	R^2	k_2 ($g.mg^{-1}.min^{-1}$)	q_e ($mg.g^{-1}$)	R^2	k_{id} ($mg.g^{-1}.min^{-0.5}$)	C_{id} ($mg.g^{-1}$)	R^2
TR	0.044	2.64E-3	0.982	60.134	0.981	1	3.75E-4	0.978	0.975
CG-H3G	0.150	0.386	0.870	0.947	0.964	0.999	0.021	0.806	0.870

3.4 Adsorption Isotherm

In this study, the Langmuir and Freundlich models were used to understand the bio-adsorption process of the TR and CG-H3G dyes on the surface of CS. The linear forms and isothermal parameters are presented in Table 4.

Table 4: Isotherm model of the Langmuir and Freundlich isotherms

Isotherm model	Parameters	Linear equation	Plot	Ref.	Eq. No.
Langmuir $q_e = \frac{k_L.\ C_e}{1 + q_m.C_e}$	k_L ($L.mg^{-1}$) qm ($mg.g^{-1}$)	$\frac{C_e}{q_e} = \left(\frac{1}{q_m}\right)C_e + \frac{1}{k_L q_m}$	$\left(\frac{C_e}{q_e}\right)$ *vs* C_e	[41]	(8)
Freundlich $q_e = k_F C_e^{\frac{1}{n}}$	k_F ($mg.g^{-1}$) ($L.mg^{-1}$)]$^{1/n}$ n	$ln\ q_e = ln\ k_F + \left(\frac{1}{n}\right) ln\ C_e$	$ln\ q_e$ *vs* $ln\ C_e$	[42]	(9)

The model of Langmuir is proposed to present the adsorption of molecules of adsorbate on a homogeneous solid surface with the formation of a single layer [43]. The model of Freundlich is an empirical model developed to represent the sorption of several compounds on heterogeneous surface sites of different affinities [44]. The values of the Langmuir and Freundlich model parameters are presented in Table 5. Graphic representation of the equilibrium isotherm, Langmuir and Freundlich model are presented in Fig. 12.

Table 5: Freundlich and Langmuir parameters (T = 22°C)

Dyes	Freundlich			Langmuir		
	k_F (mg.g^{-1}) (L.mg^{-1})$^{1/n}$	n	R^2	k_L (L.mg^{-1})	q_m (mg.g^{-1})	R^2
TR	3.195	1.732	0.924	0.112	29.412	0.935
CG-H3G	1.147	4.163	0.891	0.288	3.694	0.999

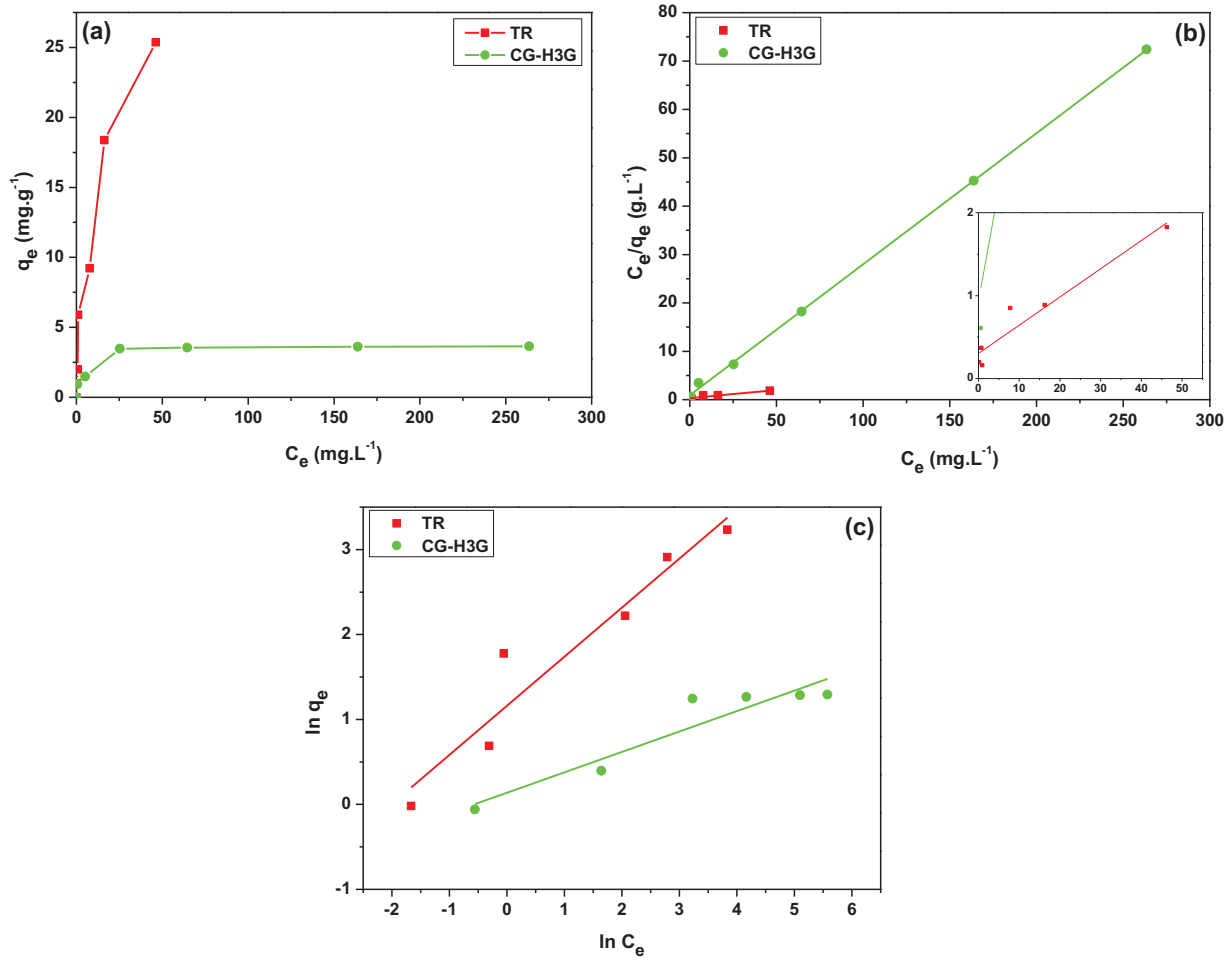

Figure 12: Graphic representation: (a) Equilibrium isotherm, (b) Langmuir and (c) Freundlich model (T = 22°C)

From Table 5, one can observe that the correlation coefficient of the Langmuir model for the two dyes is greater than that of the Freundlich model. This observation gives an indication that the Langmuir model is more adequate for presenting the adsorption process of TR and CG-H3G dyes on cockleshells. Moreover, it can be said that the TR and CG-H3G dyes are retained on a homogeneous surface with the formation of a single layer without interaction between them [40].

The Freundlich model constants also lead to conclude that the homogeneity or the heterogeneity of the surface depends on the value of n. Thus, when the value of n is greater than 1 ($n > 1$), this indicates that the system fixing the solute on the solid surface is homogeneous. However, when the value of n is lower than 1 ($n < 1$) the system is heterogeneous [45]. According to Table 5, the value of $n > 1$, so the retention system of TR and CG-H3G molecules on the solid CS surface is homogeneous.

3.5 Thermodynamic Studies

This part of this work is very important to know the adsorption process of TR and CG-H3G dyes on cockleshell powder in the 22°C–61°C temperature range, also giving information on thermodynamic parameters such as: enthalpy, entropy and Gibbs energy. The thermodynamic parameters are represented by the following equations [46]:

$$\Delta G = -RT\ ln\ kd \tag{5}$$

$$\Delta G = \Delta H - T\Delta S \tag{6}$$

$$ln\ k_d = -\frac{\Delta H}{R} \times \frac{1}{T} + \frac{\Delta S}{R} \tag{7}$$

With T (K), R (8.31 j.mol^{-1}.K^{-1}) and k_d of (qe/C_e; L/g) representing respectively the absolute temperature (K), the constant of the perfect gases and the distribution coefficient. The thermodynamic parameters: enthalpy and entropy are obtained by the slope and intersection of the linear line of $ln\ k_d$ as a function of *(1/T)* shown in Fig. 13. The results for the thermodynamic parameters are presented in Table 6.

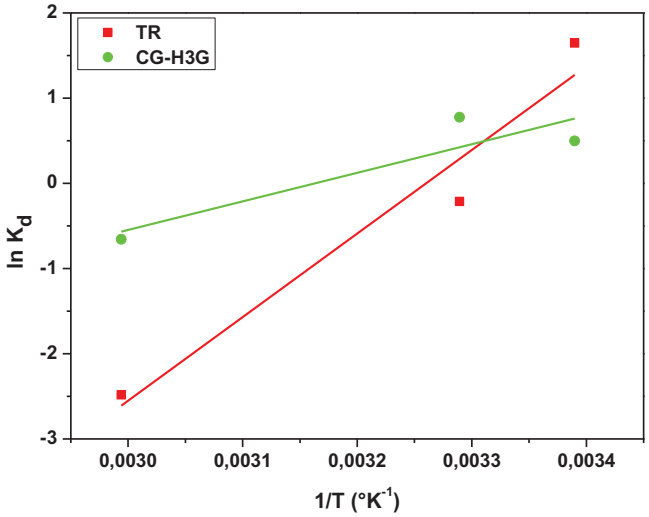

Figure 13: Van't Hoff graph of TR and CG-H3G bio-adsorption

Based on the thermodynamic parameters of dye TR and CG-H3G shown in Table 6, it can be observed that the enthalpy value is negative, indicating that the reaction between adsorbent and adsorbate is exothermic [47]. The negative value of the entropy confirms the decrease of the random character at the

solid interface–solute [47]. The negative values of the Gibbs energy in the 22°C and 31°C temperatures range reveal that bio-adsorption is spontaneous [48] except at the temperature of 61°C at which the reaction between TR, CG-H3G and the bio-adsorbent (CS) is non-spontaneous as the Gibbs energy value is positive.

Table 6: Thermodynamic parameters of bio-adsorption process of TR and CG-H3G onto Cockle shells

Dye	Thermodynamic parameters			
	T (°C)	ΔG° ($kJ.mol^{-1}$)	ΔS° ($kJ.mol^{-1}.K^{-1}$)	ΔH° ($kJ.mol^{-1}$)
TR	22	−3.12211	−0.26575	−81.51836
	31	−0.73036		
	61	7.24214		
CG-H3G	22	−1.86463	−0.08808	−27.84823
	31	−1.07191		
	61	1.57049		

4 Binary System

Industrial textile waste is responsible for the production of many pollutants, such as dyes of various shapes and colors, with a pH between 6 and 8. In our research we examined the bio-adsorption process of a mixture of two dyes (TR + CG-H3G) at a concentration of 10 mg/L for each dye by the bio-adsorbent cockle shell in the ratio of 10 g/L at a pH similar to industrial textile waste (pH = 6.04).

Fig. 14 illustrates the adsorption capacity of TR and CG-H3G dyes in single and binary systems.

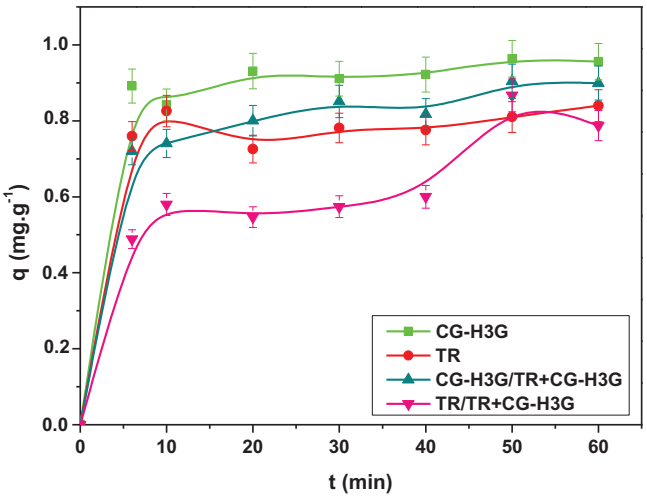

Figure 14: Affinity of TR and CG-H3G onto cockle shells ($C_{0\ TR,\ CG\text{-}H3G}$ = 10 mg/L, T = 22°C, r = 10 g/L, W = 300 rpm, pH = 6.04)

Fig. 14 shows that the adsorption capacity of the CG-H3G dye in the binary mixture is less than that of the single system. Also, there is a reduction in the adsorption of the dye TR in the binary system compared to

the single system. This observation suggests that this can be attributed to the great competition between the molecules of the TR and CG-H3G in the binary system.

4.1 Relative Adsorption and Selectivity

Selectivity plays a crucial role in the selection criteria of a bio-adsorbent to eliminate industrial releases of dyes, which are essentially pollutants. To assess selectivity in a binary system, it is essential to refer to the following relationships [49]:

$$R_a = \frac{[q]_b}{[q]_s} \tag{8}$$

$$S = \frac{(R_a)_{P1}}{(R_a)_{P2}} \tag{9}$$

With: R_a, S–relative adsorption and selectivity; $[q]_s$, $[q]_b$–the adsorption capacity of pollutant (P) in a single and binary system.

Based on Fig. 15a, it is evident that the relative adsorption of the CG-H3G dye is more stable than that of the TR dye. This shows that the CG-H3G dye has an impact on the TR dye adsorption process.

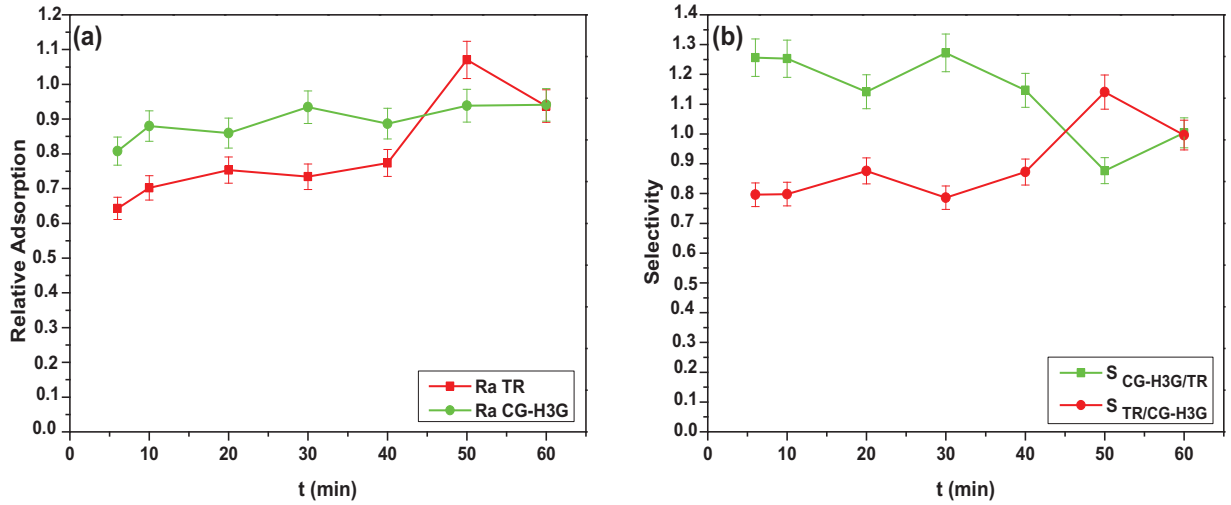

Figure 15: Relative adsorption and selectivity of TR and CG-H3G dyes onto cockle shells ($C_{0\ TR,\ CG\text{-}H3G}$ = 10 mg/L, T = 22°C, r = 10 g/L, W = 300 rpm, pH = 6.04)

Fig. 15b highlights the selectivity of the mixture of the two dyes TR and CG-H3G. Therefore, the selectivity of the CG-H3G dye gradually decreases to 50 min and then increases. However, its value is still higher than the selectivity effect of the TR dye in the binary system. Therefore, the CG-H3G dye has a preference for selectivity over the TR dye under the operating conditions used.

However, the dye CG-H3G therefore presents a preference in terms of selectivity compared to the dye TR in the interval of 6 to 45 min. At a time of 45 to 60 min, the dye TR becomes more selective than CG-H3G.

5 Conclusion

The results of this study find out that the cockleshell powder (CS) has the ability to adsorb and remove Terasil Red dye (TR) and Cibacron Green H3G (CG-H3G). The experimental results show that the

adsorption capacity is related to the following effects: contact time, dose of the adsorbent, initial concentration of TR and CG, and temperature of the medium. The bio-adsorption process was studied at a well-determined time equal to one hour. The experimental equilibrium data are well correlated with the linear forms of the Langmuir, Freundlich, and isothermal models. The Langmuir model satisfactorily predicted the isothermal data. Similarly, efficient modelling and description of kinetic data were carried out using pseudo-first order, pseudo-second order and intra-particle diffusion models. The pseudo-second-order model was most effective in predicting kinetic data. Thermodynamic studies of TR and CG-H3G dyes show that the process of bio-adsorption of TR and CG-H3G dyes is exothermic, spontaneous in the range of 22°C–31°C with the random character decreasing at the solid-solute interface during the bio-adsorption process. The selectivity of the cockleshell surface under operating conditions is highlighted by the study of selectivity, showing that the CG-H3G dye is more selective than the TR dye in the single system and binary system in the range of 6 to 45 min.

Acknowledgement: This work was supported by the University Salah Boubnider-Constantine 3 (Algeria).

Funding Statement: The authors received no specific funding for this study.

Author Contributions: Zakaria Laggoun (conceptualization, data analysis and graphs plotting); Amel Khalfaoui (writing manuscript); Kerroum Derbal (revised and correction of final manuscript); Amira Fadila Ghomrani (conceptualization, data analysis); Abderrezzaq Benalia (revised and correction of final manuscript) and Antonio Pizzi (revised and correction of final manuscript). All authors reviewed the results and approved the final version of the manuscript.

Availability of Data and Materials: The data that support the findings of this study are available on request from the corresponding author.

Ethics Approval: Not applicable.

Conflicts of Interest: The authors declare no conflicts of interest to report regarding the present study.

References

1. Sriram G, Bendre A, Mariappan E, Altalhi T, Kigga M, Ching YC, et al. Recent trends in the application of metal-organic frameworks (MOFs) for the removal of toxic dyes and their removal mechanism–a review. Sus Mater Tech. 2022;31(11):e00378. doi:10.1016/j.susmat.2021.e00378.
2. Haleem A, Shafiq A, Chen S-Q, Nazar M. A comprehensive review on adsorption, photocatalytic and chemical degradation of dyes and nitro-compounds over different kinds of porous and composite materials. Molecules. 2023;28(3):1081. doi:10.3390/molecules28031081.
3. Anisuzzaman SM, Joseph CG, Pang CK, Pang CK, Affandi NA, Maruja SN, et al. Current trends in the utilization of photolysis and photocatalysis treatment *processes* for the remediation of dye wastewater: a short review. Chem Eng. 2022;6(4):58. doi:10.3390/chemengineering6040058.
4. Ahmad T, Manzar M, Khan S, Kazi IW, Mu'azu ND, Ullah N. Synthesis and adsorptive performance of a novel triazine core-containing resin for the ultrahigh removal of malachite green from water. Arab J Sci Eng. 2022;48(7):8571–84. doi:10.1007/s13369-022-07015-w.
5. Al-Tohamy R, Ali SS, Li F, Okasha KM, Mahmoud YAG, Elsamahy T, et al. A critical review on the treatment of dye-containing wastewater: ecotoxicological and health concerns of textile dyes and possible remediation approaches for environmental safety. Eco Env Saf. 2022;231(2):113160. doi:10.1016/j.ecoenv.2021.113160.
6. Dobrosz-Gómez I, Quintero-Arias J-D, Gómez-García M-Á. Coagulation-Flocculation—Fenton-Neutralization sequential process for the treatment of industrial effluent polluted with AB194 dye. Case Stud Chem Env Eng. 2024;9(20):100720. doi:10.1016/j.cscee.2024.100720.

7. Singh S, Prajapati A, Chakraborty J, Mondal M. Adsorption potential of biochar obtained from pyrolysis of raw and torrefied Acacia nilotica towards removal of methylene blue dye from synthetic wastewater. Biomass Conv Bioref. 2021;13(7):6083–104. doi:10.1007/s13399-021-01645-0.
8. Hasnaoui A, Chikhi M, Balaska F, Seraghni W, Boussemghoune M, Dizge N. Electrocoagulation employing recycled aluminum electrodes for methylene blue remediation. Desalin Water Treat. 2024;319(42):100453. doi:10.1016/j.dwt.2024.100453.
9. Taqui SN, S MC, Khatoon BA, Soudagar M, Yunus Khan ME, Mujtaba TM, et al. Sustainable adsorption method for the remediation of malachite green dye using nutraceutical industrial fenugreek seed spent. Biomass Conv Bioref. 2023;13(10):9119–30. doi:10.1007/s13399-021-01827-w.
10. Pavan Kumar GVSR, Malla KA, Yerra B, Srinivasa Rao K. Removal of Cu(II) using three low-cost adsorbents and prediction of adsorption using artificial neural networks. Appl Water Sci. 2019;9(3):44. doi:10.1007/s13201-019-0924-x.
11. Mondal NK, Chakraborty S. Adsorption of Cr(VI) from aqueous solution on graphene oxide (GO) prepared from graphite: equilibrium, kinetic and thermodynamic studies. Appl Water Sci. 2020;10(2):61. doi:10.1007/s13201-020-1142-2.
12. Matabola K, Teboho M, Sikhwivhilu K, Mokhothu TH, Mochane MJ. Poly(vinyl alcohol) (PVA)-based nanofibers materials for azo dye adsorption: an overview. Inter J Env Sci Tech. 2022;20(6):7029–54. doi:10.1007/s13762-022-04666-y.
13. Lu Y, Cai Y, Zhang S, Zhuang L, Hu B, Wang S, et al. Application of biochar-based photocatalysts for adsorption-(photo) degradation/reduction of environmental contaminants: mechanism, challenges and perspective. Biochar. 2022;4(1):45. doi:10.1007/s42773-022-00173-y.
14. Bhutto AA, Baig JA, Sirajuddin, Kazi TG, Alvarez RS, Akhtar K. Biosynthesis and analytical characterization of iron oxide nanobiocomposite for in-depth adsorption strategy for the removal of toxic metals from drinking water. Arab J Sci Eng. 2023;48(6):7411–24. doi:10.1007/s13369-022-07477-y.
15. Si Y, Li J, Cui B, Tang D, Yang L, Murugadoss V, et al. Janus phenol-formaldehyde resin and periodic mesoporous organic silica nanoadsorbent for the removal of heavy metal ions and organic dyes from polluted water. Adv Comp Hyb Mater. 2022;5(2):1–16. doi:10.1007/s42114-022-00446-x.
16. Baatache O, Derbal K, Benalia A, Aberkane I, Guizah QE, Khalfaoui A, et al. Valorization of pine cones (*Pinus nigras*) for industrial wastewater treatment and crystal violet removal: a sustainable approach based on bio-coagulants and a bio-adsorbent. Water. 2024;16(2):260. doi:10.3390/w16020260.
17. Laggoun Z, Khalfaoui A, Benalia A, Ghomrani AF, Bouchareb R, Mahfouf A, et al. Application of response surface design for optimization of direct red dye biosorption onto cockleshells. Appl Sci. 2023;13(22):12333. doi:10.3390/app132212333.
18. Rashid R, Shafiq I, Akhter P, Iqbal MJ, Hussain M. A state-of-the-art review on wastewater treatment techniques: the effectiveness of adsorption method. Env Sci Poll Res. 2021;28(8):9050–66. doi:10.1007/s11356-021-12395-x.
19. Kebir M, Tahraoui H, Chabani M, Trari M, Noureddine N, Assadi AA, et al. Water cleaning by a continuous fixed-bed column for Cr(VI) eco-adsorption with green adsorbent-based biomass: an experimental modeling study. Process. 2023;11(2):363. doi:10.3390/pr11020363.
20. Combes C, Miao B, Bareille R, Rey C. Preparation, physical–chemical characterisation and cytocompatibility of calcium carbonate cements. Biomaterials. 2006;27(9):1945–54. doi:10.1016/j.biomaterials.2005.09.026.
21. Daud Z, Abubakar MH, Kadir AA, Abdul Latiff AA, Awang H, Abdul Halim A, et al. Batch study on COD and ammonia nitrogen removal using granular activated carbon and cockle shells. Int J Eng, Transact A: Basics. 2017;30(7):937–44. doi:10.5829/ije.2017.30.07a.02.
22. Mohd Zain NB, Md Salleh NJ, Hisamuddin NF, Hashim S, Abdullah NH. Adsorption of phosphorus using cockle shell waste. Indus Dom Waste Man. 2022;2(1):30–8. doi:10.53623/idwm.v2i1.81.
23. Velázquez-Castillo R, Reyes-Gasga J, García-Gutierrez DI, Jose-Yacaman M. Nanoscale characterization of nautilus shell structure: an example of natural self-assembly. J Mater Res. 2006;21(6):1484–9. doi:10.1557/jmr.2006.0190.

24. Shafiu Kamba A, Ismail M, Tengku Ibrahim TA, Zakaria ZAB. Synthesis and characterisation of calcium carbonate aragonite nanocrystals from cockle shell powder (*Anadara granosa*). J Nano. 2013;2013(1):1–9. doi:10.1155/2013/398357.
25. Hoque1 ME, Shehryar1 M, Nurul Islam KM. Process and characterization of cockle shell calcium carbonate ($CaCO_3$) bioceramic for potential application in bone tissue engineering. J Mater Sci Eng. 2013;2(4):1000131. doi:10.4172/2169-0022.1000132.
26. Jabar JM, Odusote YA, Alabi KA, Ahmed IB. Kinetics and mechanisms of Congo-red dye removal from aqueous solution using activated *Moringa oleifera* seed coat as adsorbent. Appl Water Sci. 2020;10(6):136. doi:10.1007/s13201-020-01221-3.
27. Azeez RA, Al-Zuhairi FKI. Biosorption of dye by immobilized yeast cells on the surface of magnetic nanoparticles. Alex Eng J. 2022;61(7):5213–22. doi:10.1016/j.aej.2021.10.044.
28. Xiao W, Garba ZN, Sun S, Lawan I, Wang L, Lin M, et al. Preparation and evaluation of an effective activated carbon from white sugar for the adsorption of rhodamine B dye. J Cle Pro. 2020;253:119989. doi:10.1016/j.jclepro.2020.119989.
29. Bajaber MA, Anjum MN, Ibrahim M, Farooq T, Ahmad MN, Ul Abideen Z. Synthesis and characterization of hydroxyethyl cellulose grafted with copolymer of polyaniline and polypyrrole biocomposite for adsorption of dyes. Molecules. 2022;27(23):8238. doi:10.3390/molecules27238238.
30. Thommes M, Kaneko K, Neimark AV, Olivier JP, Rodriguez-Reinoso F, Rouquerol J, et al. Physisorption of gases, with special reference to the evaluation of surface area and pore size distribution (IUPAC Technical Report). Pure Appl Chem. 2015;87(9–10):1051–69. doi:10.1515/pac-2014-1117.
31. Khalfaoui A, Benalia A, Selama Z, Hammoud A, Derbal K, Panico A, et al. Removal of chromium (VI) from water using orange peel as the biosorbent: experimental, modeling, and kinetic studies on adsorption isotherms and chemical structure. Water. 2024;16(5):742. doi:10.3390/w16050742.
32. Khalfaoui A, Benalia A, Laggoun Z, Bouchareb R, Zaamta I, Melloula R, et al. Effective synthesis and application of artichoke and orange peels-based bio-sorbents for Ketoprofen removal from wastewater: process optimization using Factorial methodology. Desalin Water Treat. 2024;317:100197. doi:10.1016/j.dwt.2024.100197.
33. Zamouche M, Habib A, Saaidia K, Bencheikh Lehocine M. Batch mode for adsorption of crystal violet by cedar cone forest waste. SN Appl Sci. 2020;2(2):198. doi:10.1007/s42452-020-1976-0.
34. Kavci E, Erkmen J, Bingöl MS. Removal of methylene blue dye from aqueous solution using citric acid modified apricot stone. Chem Eng Coms. 2023;210(2):165–80. doi:10.1080/00986445.2021.2009812.
35. Bouhedda M, Lefnaoui S, Rebouh S, Yahoum MM. Predictive model based on Adaptive Neuro-fuzzy Inference System for estimation of Cephalexin Adsorption On The Octenyl Succinic Anhydride starch. Chemometr Intell Lab Syst. 2019;193(5):103843. doi:10.1016/j.chemolab.2019.103843.
36. Baouch Z, Kamel Ismet B, Bouras B. Adsorption of different dyes from aqueous solutions using organo-clay compposites. Phys Chem Res. 2020;8:767–87. doi:10.22036/pcr.2020.234691.1787.
37. El-Desouky MG, El-Bindary MA, El-Bindary AA. Effective adsorptive removal of anionic dyes from aqueous solution. Veit J Chem. 2021;59(3):341–61. doi:10.1002/vjch.202000184.
38. Al-Zoubi H, Zubair M, Manzar MS, Manda AA, Blaisi NI, Qureshi A, et al. Comparative adsorption of anionic dyes (Eriochrome Black T and Congo Red) onto jojoba residues: isotherm, kinetics and thermodynamic studies. Arab J Sci Eng. 2020;45(9):7275–87. doi:10.1007/s13369-020-04418-5.
39. Mtavangu SG, Mahene W, Machunda RL, Machunda RL, Bruggen BV, Njau KN, et al. Cockle (*Anadara granosa*) shells-based hydroxyapatite and its potential for defluoridation of drinking water. Results Eng. 2022;13(4):100379. doi:10.1016/j.rineng.2022.100379.
40. Shoaib AGM, Sikaily AE, Ragab S, Masoud MS, Ramadan MS. Starch-grafted-poly(acrylic acid)/*Pterocladia capillacea*-derived activated carbon composite for removal of methylene blue dye from water. Biomass Conv Bioref. 2022;14(21):27189–209. doi:10.1007/s13399-022-03382-4.
41. Ahmadi S, Mohammadi L, Rahdar A, Rahdar S, Dehghani R, Igwegbe CA, et al. Acid dye removal from aqueous solution by using neodymium(III) oxide nanoadsorbents. Nanomaterials. 2020;10(3):556. doi:10.3390/nano10030556.

42. Musah M, Azeh Y, Mathew J, Musah M, Azeh Y, Mathew JT, et al. Adsorption kinetics and isotherm models: a review. CaJoST. 2022;4(1):20–6. doi:10.4314/cajost.v4i1.3.
43. Syafiuddin A, Salmiati S, Jonbi J, Fulazzaky MA. Application of the kinetic and isotherm models for better understanding of the behaviors of silver nanoparticles adsorption onto different adsorbents. J Env Man. 2018;218:59–70. doi:10.1016/j.jenvman.2018.03.066.
44. Ammendola P, Raganati F, Chirone R. CO_2 adsorption on a fine activated carbon in a sound assisted fluidized bed: thermodynamics and kinetics. Chem Eng J. 2017;322(5):302–13. doi:10.1016/j.cej.2017.04.037.
45. Neolaka YAB, Lawa Y, Naat J, Lalang AC, Widyaningrum BA, Ngasu GF, et al. Adsorption of methyl red from aqueous solution using Bali cow bones (*Bos javanicus domesticus*) hydrochar powder. Res In Eng. 2023; 17(16):100824. doi:10.1016/j.rineng.2022.100824.
46. da Costa TB, da Silva MGC, Vieira MGA. Crosslinked alginate/sericin particles for bioadsorption of ytterbium: equilibrium, thermodynamic and regeneration studies. Int J Bio Mac. 2020;165:1911–23. doi:10.1016/j.ijbiomac.2020.10.072.
47. Nti Kani AN, Dovi E, Mpatani FM, Li Z, Han R, Qu L. Tiger nut residue as a renewable adsorbent for methylene blue removal from solution: adsorption kinetics, isotherm, and thermodynamic studies. Desalin Water Treat. 2020;191:426–37. doi:10.5004/dwt.2020.25735.
48. Al-Hazmi AAG, El-Zahhar AA, El-Desouky MG, El-Bindary MA, El-Bindary AA. Efficiency of Fe_3O_4 @ZIF-8 for the removal of Doxorubicin from aqueous solutions: equilibrium, kinetics and thermodynamic studies. Env Tech. 2024;45(4):731–50. doi:10.1080/09593330.2022.2121181.
49. Mezenner NY, Bensaadi Z, Lagha H, Bensmaili A. Etude de l'adsorption d'une mixture de composes bio-récalcitrants en milieu aqueux. LARHYSS J. 2012;9(2):7–16.